Determination of the Response Amplitude Operator of a tidal turbine as a spectral transfer function

B. Gaurier, G. Germain, and J. V. Facq

Abstract—**A transfer function determination method is proposed in this study to predict the unsteady fluctuations of the performance of a tidal turbine model. This method is derived from the Response Amplitude Operator (RAO) applied in the offshore industry to predict linear wave-induced loads on large structures. It is based on a spectral approach and requires the acquisition of a turbine parameter (e.g. torque, thrust, power or root-blade force) in synchronization with an upstream flow velocity measurement. On the frequency range where the causality between these two signals is proven, the transfer function is established using the ratio between the cross-spectral density and the spectral density of the incoming velocity. The linearity is verified using the coherence function, which shows validity for the turbine power in the lowest frequencies only. This transfer function is then used to reconstruct the power fluctuations which is compared to the recorded one for a particular flow condition with bathymetry generated turbulence. The result shows the dependence on the accurate location of the velocity measurement point used for the reconstruction. This point must exactly correspond to the expected turbine location, i.e. where the turbine response needs to be processed. Bearing in mind its limits, the method can be used to predict the loadings of extreme events on the turbine structure and the performance variations corresponding to the unsteady characteristics of a turbulent flow, for a better grid integration.**

Index Terms—**experimental trials, Response Amplitude Operator, tidal turbine, transfer function, turbulence, wave-current interactions**

I. Introduction

CURRENTLY, the biggest problem with energy extraction in the marine environment is the complex and diverse flow conditions, which also makes deployment and survival of a tidal turbine a challenge for developers [1], [2]. To enable tidal turbine to become commercially viable, device components must be able to withstand substantial forces with significant spatial and temporal variations. Knowledge of normal operational loads, extreme operational loads and the characteristics of load fluctuations is required to minimise the probability of device failure due to overloading and fatigue [3]. The electricity generation cost reduction also involves a better resource assessment of the commercial sites and the limitation of energy losses [4]. As explained by [5] for wind turbines, variability in the power output introduces a challenge for the integration of large amounts of wind (or tidal) energy in an electricity grid. Power output variability is inherently present due to the unsteady characteristics of the flow, from which the turbines extract kinetic energy. The necessary fill-in power to compensate for the power output variability and the need for stronger components increase the global cost of this kind of renewable energy.

Major works combining in-situ measurements, experimental and numerical developments are being carried out but still suffer today from many limitations due to the strong assumptions resulting from the lack of knowledge of the response of the tidal turbine under extreme conditions. A more precise resource assessment can be obtained by a better environment knowledge as performed by [6] accounting for the turbulence, but also by taking into account the specificity of the used turbines. It is then necessary to be able to characterize the response of the machines for realistic operating conditions in order to define as much as possible the most representative and precise transfer functions linked to the flow characteristics. Energy production can also be optimized by identifying the energy losses encountered under such operating conditions. These data can be obtained after full-scale deployment but with high risks and investment costs. In order to limit the risk, lab-scale experiments can be conducted to reproduce realistic ocean conditions and to quantify the magnitude of these sub-surface forces prior to the full-scale deployment of a device.

From various experimental databases obtained in the wave and current circulating tank of IFREMER, we present a spectral method to determine the generic transfer function of a 1/20 scaled model tidal turbine, for several realistic operating conditions. Various flow configurations is investigated: high turbulence rate encountered on sites with strong currents (1.5 % to 15 %

Manuscript received December 22nd, 2021, published 15 September 2022.

The research leading to these results has received funding from the European Union Horizon 2020 Framework Program (H2020) for MaRINET2 project under grant agreement no 731084 and for RealTide project under grant agreement no 727689. This project was partly financially supported by the French government, IFREMER and the region Hauts-de-France in the framework of the project CPER 2015-2020 MARCO

B. Gaurier, G. Germain and J. V. Facq are at the French Research Institute for Exploitation of the Sea (IFREMER), Centre Manche – Mer du Nord, 62 200 Boulogne-sur-mer, France (e-mail: bgaurier@ifremer.fr, ggermain@ifremer.fr, jvfacq@ifremer.fr).

Digital Object Identifier: https://doi.org/10.36688/imej.5.151-160

of turbulence intensity with current up to $1.2\,\mathrm{m/s}$), presence of large vortex structures, and combined wave and current interactions. The experimental set-up is first described and the transfer function determination methodology is detailed. Results obtained for the various flow conditions previously cited are compared and a discussion is leaded on the accuracy of the method. A comparison of the recorded and reconstructed power fluctuations using this transfer function is carried out under flow conditions with bathymetry generated turbulence before to conclude on the limitations and possibilities of such a method.

II. Materiel and methods

This first section is divided in two parts with the description of the experimental set-up and the methodology leading to the transfer function determination.

A. Experimental set-up

The experimental datasets used in this study correspond to trials which have all been carried out in the wave and current flume tank of IFREMER at Boulogne-sur-mer, France (Fig. 1). Dimensions of the testing area are $18\,\mathrm{m}$ long, $4\,\mathrm{m}$ wide and $2\,\mathrm{m}$ deep. Two pumps generate a turbulent flow with a speed range between 0.1 to $2.2\,\mathrm{m/s}$. The turbulence intensity can be reduced by the use of a flow straightener, leading to a turbulence intensity of $I_\infty \simeq 1.5\,\%$. When the flow straightener is removed, the intensity reaches values of $I_\infty \simeq 15\,\%$. A wavemaker can be positioned in the upper part of the testing area to create wave with or against the current. Because this wavemaker is intrusive, it modifies the vertical velocity profile as well as the turbulence intensity. More information about the flume tank can be found in [7].

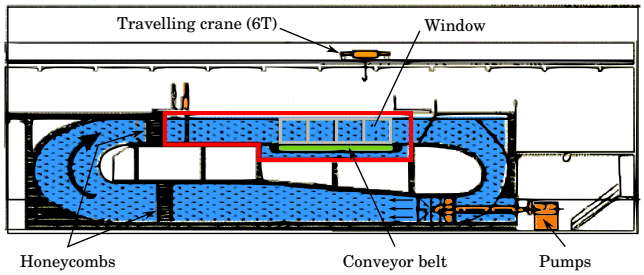

Fig. 1. Schematic of the wave and current flume tank of IFREMER, with the testing area highlighted in red line

Two databases are used, based on the same test set-up represented on Fig. 2, but with various inflow conditions: flow speeds, velocity profiles, turbulence intensities and wave-current combinations. The same turbine model (Fig. 3) is fixed in the very centre of the testing area and a flow measurement is taken using a Laser Doppler Velocimeter (LDV) located at a distance d upstream of the rotor. The different inflow conditions are summarized in table I for the two databases. In this table, U_∞ and I_∞ stand for the far upstream velocity and turbulence intensities respectively, and f_w is the wave frequency when available. References to previous works where these databases were initially used are given as well.

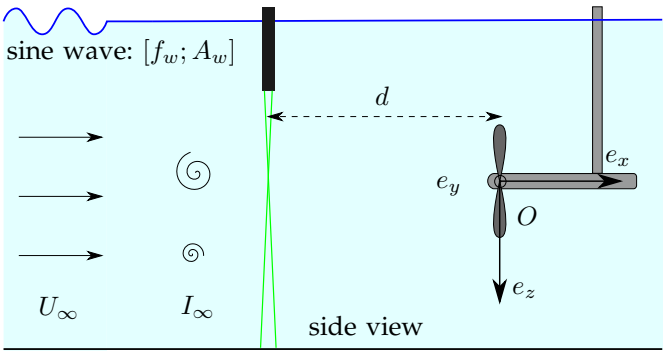

Fig. 2. Schematic of the test set-up in the wave and current flume tank. It includes the Laser Doppler Velocimeter (LDV) located at a distance d from the turbine model and successively used with current only: two magnitudes U_∞ and two turbulent rates I_∞ and with current and regular wave: frequency f_w and amplitude A_w. The acquisition of the upstream flow velocity by the LDV is always carried out in synchronization with the turbine parameters.

TABLE I
INFLOW CONDITIONS OF THE DATABASES USED IN THIS STUDY

Name	U_∞ [m/s]	I_∞ [%]	f_w [Hz]	Ref.
Database A	0.6 to 1.2	1.5 and 15	no wave	[8]
Database B	0.8 and 1.0	1.5	0.5 to 0.7	[9], [10]

The three-bladed horizontal-axis turbine model has been developed by IFREMER and is shown on Fig. 3. The turbine is $0.724\,\mathrm{m}$ in diameter (D) and is speed-controlled using a motor speed-control unit. The blades are designed based on a NACA 63-418 profile. This model is equipped with a dedicated load-cell in each blade root and with a torque and thrust transducer measuring forces on the main rotation axis of the rotor (Fig. 4). This waterproof transducer is positioned upstream of the seals of the machine to prevent measuring friction effects. The shielded cables coming from these transducers are routed through a slip-ring enabling the free rotation of the cables while prevent their entanglement. These low voltage signals are amplified by an electronic signal processing unit, located outside of the turbine and on the dry. The signal amplification is not possible inside the turbine because of the restricted volume. However, the shielded cables and the slipring quality limit the noise in the low-voltage analogue signals. The motor shaft is connected to the turbine shaft through a motor-gearbox facilitating the acquisition of suitable torque and rotation speed ratings.

All signals are acquired using National Instruments hardware and in-house electronics developed by IFREMER staff. The signals are sampled at a frequency of $128\,\mathrm{Hz}$. The acquisition duration changes depending on the turbulence intensity for the convergence of the results. This last parameter is summarized in table II. As explained before, because the wavemaker is intrusive, the acquisition duration is longer even if the turbulence intensity is low for database B (see table I). The turbulence rate is actually $I_\infty \simeq 10\,\%$ at the turbine depth when the wavemaker is inside the water [9].

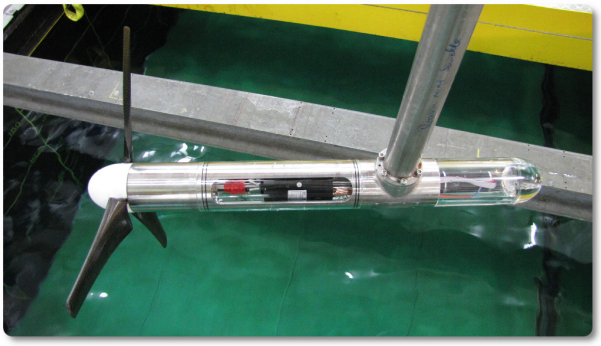

Fig. 3. Picture of the turbine model outside the water. The rotor diameter is $D = 0.724\,\mathrm{m}$.

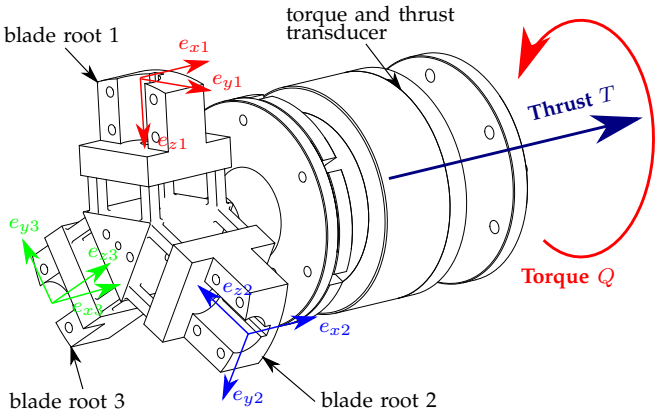

Fig. 4. Schematic of the turbine transducers: 2 forces and 3 moments are measured on each blade root as well as global torque and thrust on the main rotor axis.

Note that this turbulence rate is processed when the wavemaker is parked, i.e. with no wave and no orbital motion.

TABLE II
ACQUISITION DURATION DEPENDING ON THE INFLOW CONDITIONS. THE SAMPLING FREQUENCY IS CONSTANT AT 128 Hz.

Inflow conditions	acq. duration [s]
$I_\infty = 1.5\,\%$	180
$I_\infty = 15\,\%$	360
With wavemaker	256

According to previous results [8], [9], the designed tip speed ratio of the turbine is:

$$TSR = \frac{\omega \times R}{U_\infty} = 4 \tag{1}$$

with ω the angular frequency and R the turbine radius. This target TSR is achieved by setting the desired RPM to the motor for a given inflow velocity U_∞. In the following, all data extracted from databases A and B correspond to acquisitions while the turbine rotates at this specific designed TSR. The main other parameter extracted from the databases is the turbine power, which is classically processed from:

$$P = \omega \times Q \tag{2}$$

with Q standing for the rotor torque. Note that the rotation frequency ω is measured from the motor controller and is recorded as well as the other turbine parameters.

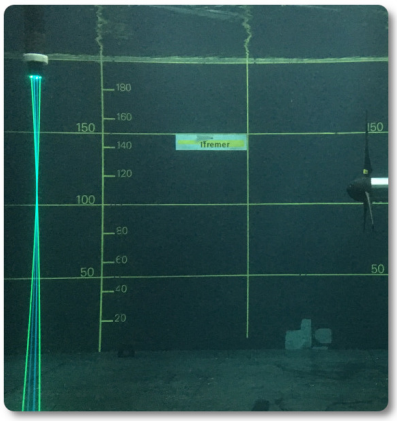

Fig. 5. LDV probe measuring the flow velocity upstream of the turbine rotor. The distance between LDV and the turbine model is $d = 2D$. Measurements are carried out at the hub height of the turbine, corresponding to the mid-depth of the water column.

The incoming velocity is measured using the LDV located at a distance $d = 2D$ upstream of the rotor and at the hub height of the turbine, corresponding to the mid-depth of the water column (Fig. 5). This facility enables velocity measurements to be taken at a single point in the flow field, with high temporal resolution. LDV is non-intrusive because the distance between the probe and the measurement point, i.e. intersection of the laser beams, is $530\,\mathrm{mm}$ into the water. The measurement volume is $2.51\,\mathrm{mm}$ long by the laser beams thickness of $0.12\,\mathrm{mm}$, which makes $V_{LDV} \simeq 0.01\,\mathrm{mm}^3$. This 2-component system is composed of 4 laser beams with 2 different wave lengths: $514\,\mathrm{nm}$ and $488\,\mathrm{nm}$. Whenever a reflecting particle entrained in the fluid passes through the measurement point, the scattered light received from the particle fluctuates in intensity. LDV makes use of the fact that the frequency of this fluctuation is equivalent to the Doppler shift between the incident and scattered light, and is thus proportional to the component of the particle velocity in the direction of the beam. The water in the tank is seeded with particles which are spherical and composed of silver coated glass. The size of particles used in the IFREMER flume tank is $10\,\mu\mathrm{m}$.

The data-rate depends on the number of particles detected by the system. In this study, the average detection frequency is typically of the order of $130\,\mathrm{Hz}$ for database A and $350\,\mathrm{Hz}$ for database B. In the following, only the streamwise component of the velocity u, i.e. following the e_x direction (Fig. 2), is considered. For the post-processing done hereafter, velocity records are interpolated and down-sampled at the same frequency than the turbine acquisitions, i.e. $f_s = 128\,\mathrm{Hz}$.

B. Response Amplitude Operator determination

The Response Amplitude Operator (RAO) is processed between the upstream flow measurement (input) and the turbine parameters (output). In this study, the output is chosen as the turbine power P (see equation 2). However, the rotor thrust or root blade forces can be selected in the same way.

The Power Spectral Density (PSD) of the velocity $u(t)$ is classically expressed by equation 3, with $\mathcal{F}$ standing for the Fast Fourier Transform, f_s the sampling frequency and n the number of acquired samples.

$$G_{uu}(f) = \frac{1}{f_s \times n} |\mathcal{F}(u(t))|^2 \tag{3}$$

PSD of the incoming velocity and of the turbine power are shown on Fig. 6, for two far-upstream velocities $U_\infty = 1.0$ and $1.2\,\mathrm{m/s}$ and for the highest turbulence intensity in the tank $I_\infty = 15\,\%$ (database A in table I). These PSDs are processed using a window length of 2^{12} points overlapping by $50\,\%$. u and P are re-phased before to process their PSDs, accounting for the distance $d = 2D$ between the LDV measurement point and the turbine rotor. The inter-correlation between both signals is calculated and the average phase lag, corresponding to the maximum of the inter-correlation, is time compensated. The classical Richardson-Kolmogorov energy cascade is clearly observed on the PSD of the velocity in the inertial range (Fig. 6a), i.e. between $f = 0.2$ and $20\,\mathrm{Hz}$, with the -5/3 energy decay. The power law is different for the turbine power (Fig. 6b), close to -11/3 as already observed by [11]–[14] and recently described by [15]. The PSD of the power is especially marked by the blade passing frequency peak, centred at $f = 5.2\,\mathrm{Hz}$ and $f = 6.2\,\mathrm{Hz}$ respectively for $U_\infty = 1.0\,\mathrm{m/s}$ and $U_\infty = 1.2\,\mathrm{m/s}$, and corresponding to three times the turbine rotation frequency. TSR is constant and equal to 4 for the two far-upstream velocities, which means the turbine rotation frequency differs for the two velocities.

In the same way, the cross-spectral density $G_{uP}(f)$ is defined by equation 4, with the over-line standing for the complex conjugate.

$$G_{uP}(f) = \frac{1}{f_s \times n} \left(\mathcal{F}(u(t)) \times \overline{\mathcal{F}(P(t))} \right) \tag{4}$$

From equations 3 and 4, the coherence function between the input velocity $u(t)$ and the turbine power $P(t)$ can be processed through equation 5.

$$C_{uP}(f) = \frac{|G_{uP}(f)|^2}{G_{uu}(f) \times G_{PP}(f)} \tag{5}$$

The coherence functions corresponding to the same flow conditions are displayed on Fig. 7. These coherence functions are quite similar for the two far-upstream velocities. As already observed by [14], the coherence function is relatively high, i.e. higher than 0.6, for the lowest frequencies. Coherence then sharply decreases between $f = 0.2$ and $1\,\mathrm{Hz}$ to fall to very low values, i.e. lower than 0.1. According to [12], [16] who performed a similar study on a single wind turbine, the rotor behaves as a low-pass filter: it ignores the small-scale fluctuations and only responds to larger coherent structures. [11] introduced a critical frequency, expressed by $f_c = U_\infty/(D/2)$ as the highest flow frequency influencing the turbine. For the highest frequencies (higher than f_c), the power appears to be insensitive to the turbulent flow structure. In our case, $f_c \simeq 3\,\mathrm{Hz}$. This is in agreement with what is observed

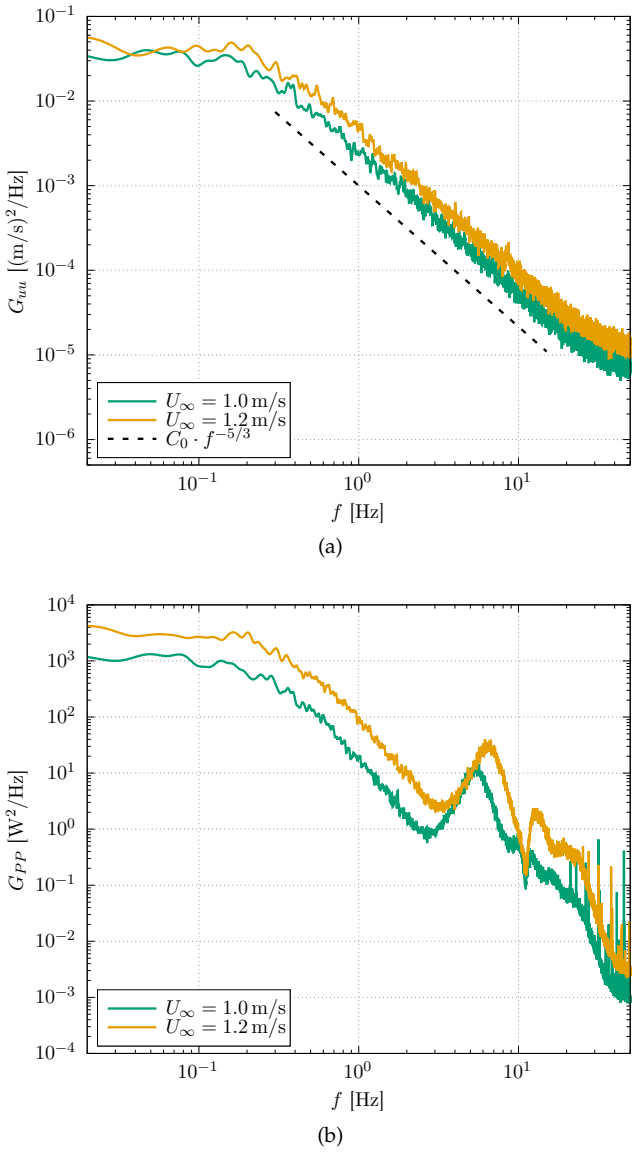

Fig. 6. Power Spectral Densities of: (a) the input velocity G_{uu} and (b) the turbine power G_{PP}, for two far-upstream velocity magnitudes $U_\infty = 1.0$ and $1.2\,\mathrm{m/s}$ and for high turbulence rate $I_\infty = 15\,\%$. The turbine rotates at the designed $TSR = 4$.

on Fig. 7. From $f = 1\,\mathrm{Hz}$, $C_{uP} \simeq 0$ means $u(t)$ and $P(t)$ are completely unrelated.

On the contrary, because $C_{uP}(f) > 0.5$ for the lowest frequencies, $P(t)$ is partially linearly related to $u(t)$. The causality between these two signals can be studied. From that point, we make the following assumption: when $C_{uP}(f) > 0.5$, a linear relation exists between u and P. In the presented example, this is true for $f \leq 0.4\,\mathrm{Hz}$. The transfer function between input and output can then be determined. This transfer function is often named Response Amplitude Operator (RAO). In the offshore industry, these RAOs are typically calculated to predict linear wave induced loads on large volume structures [17], on the basis of potential theory. In our study, the RAO is defined by equation 6, based on previous formulas 3 and 4.

$$RAO(f) = \frac{G_{uP}(f)}{G_{uu}(f)} = A(f) e^{i\varphi(f)} \tag{6}$$

From this last formula, the magnitude (i.e. modulus) $A(f)$ and phase (i.e. argument) $\varphi(f)$ of the turbine

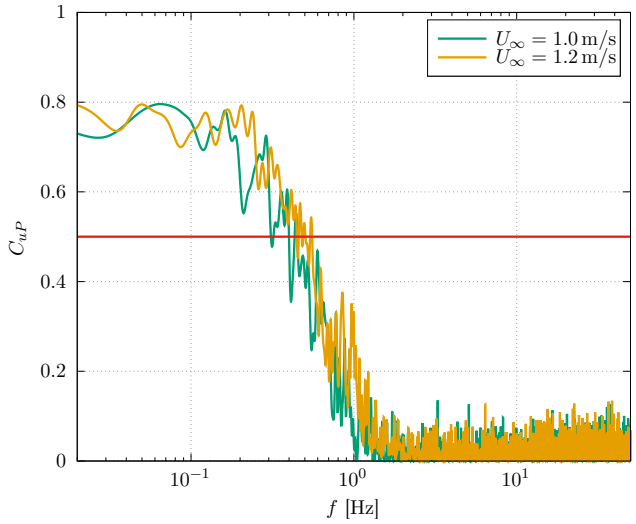

Fig. 7. Coherence functions C_{uP} between the input velocity and the turbine power for two far-upstream velocity magnitudes $U_\infty = 1.0$ and $1.2\,\mathrm{m/s}$ and for high turbulence rate $I_\infty = 15\,\%$. The red line at $C_{uP} = 0.5$ stands for the causality threshold.

transfer function can then be processed.

In the following section, we compare the RAO magnitude and phase obtained for the turbine when submitted to the different flow configurations described in section II-A.

III. Results

Magnitudes and phases of the turbine power RAOs obtained for the different flow configurations are shown on Fig. 8. For an easier comparison of the results, RAOs are presented with only one changing flow parameters by plot. The effect of the flow velocity is first presented on Fig. 8a, with $U_\infty = 1.0$ and $1.2\,\mathrm{m/s}$, from the spectra previously shown on Fig. 6. The effect of the turbulence intensity is then displayed on Fig. 8b, with $I_\infty = 1.5$ and $15\,\%$, for the same velocity magnitude $U_\infty = 1.0\,\mathrm{m/s}$. Finally the last plot (Fig. 8c) shows the results for two wave frequencies and the same combined flow velocity $U_\infty = 1.0\,\mathrm{m/s}$.

These results are plotted against a linear x-scale on the contrary to the figures presented in the previous section II-B. As shown on Fig. 7, the frequency range where the coherence function is higher than 0.5 is limited to the lowest frequencies only, i.e. always lower than $1\,\mathrm{Hz}$. This explains why a linear x-scale is chosen to display RAOs on Fig. 8.

When comparing all the results together, it clearly appears that the RAO magnitudes globally decrease when the frequency increases. The highest amplitudes are reached for the lowest frequencies, with values between 150 and $250\,\mathrm{W/(m/s)}$ for $f \simeq 0.2\,\mathrm{Hz}$. These values are in agreement with the standard-deviation ratios reported on table III: $\sigma(P)/\sigma(u) = 146$ and $219\,\mathrm{W/(m/s)}$, for $U_\infty = 1.0$ and $1.2\,\mathrm{m/s}$ respectively. On the contrary, phases are quite constant versus the frequency, with values close to $0°$ whatever the frequency. That means the turbine response always stays in phase with the velocity fluctuations.

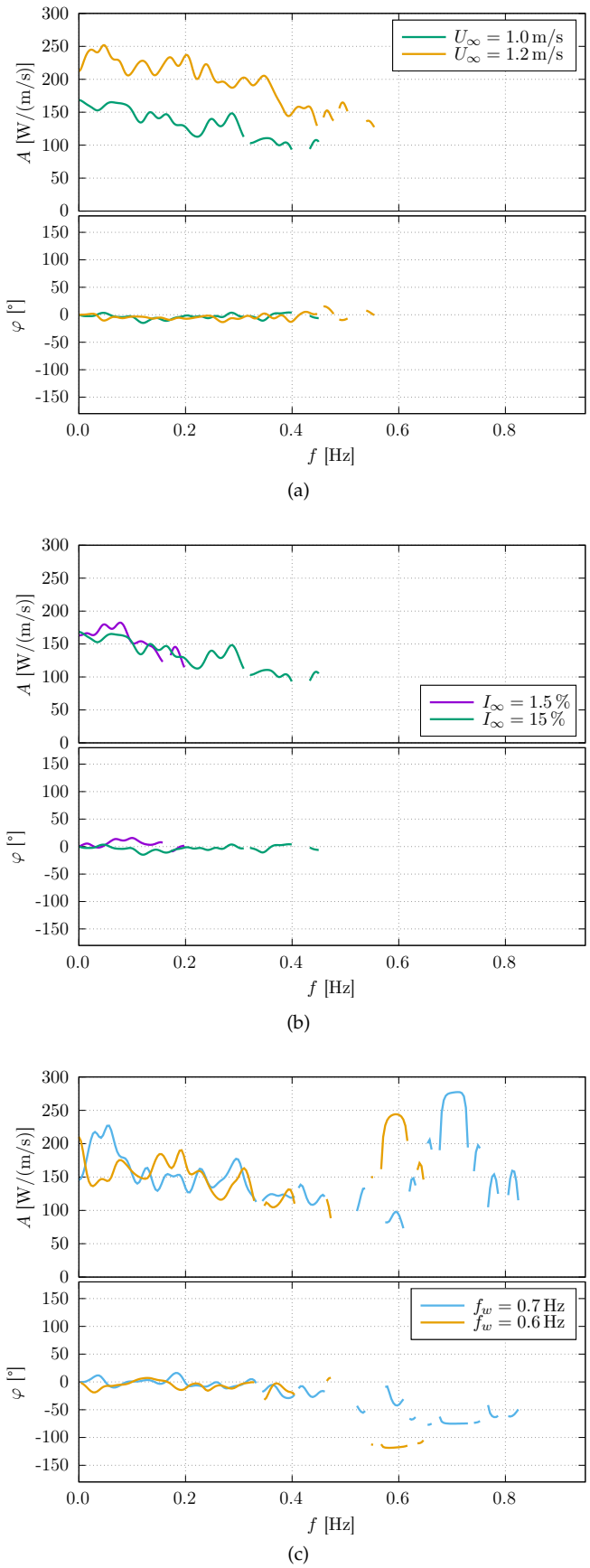

Fig. 8. Response Amplitude Operator (RAO) of the turbine power, when rotating at $TSR = 4$, for: (a) two velocity magnitudes $U_\infty = 1.0$ and $1.2\,\mathrm{m/s}$ for high turbulence rate $I_\infty = 15\,\%$, (b) two turbulence rates $I_\infty = 1.5$ and $15\,\%$ for a flow velocity $U_\infty = 1.0\,\mathrm{m/s}$ and (c) two wave and current conditions with $f_w = 0.7$ and $0.6\,\mathrm{Hz}$ for a flow velocity $U_\infty = 1.0\,\mathrm{m/s}$.

TABLE III
TIME AVERAGE AND STANDARD-DEVIATION OF THE INCOMING VELOCITY AND TURBINE POWER FOR THE HIGHEST TURBULENCE RATE $I_\infty = 15\,\%$

Inflow conditions	$\overline{P}$ [W]	$\sigma(P)$ [W]	$\overline{u}$ [m/s]	$\sigma(u)$ [m/s]
$U_\infty = 1.0\,\mathrm{m/s}$	84	19	0.96	0.13
$U_\infty = 1.2\,\mathrm{m/s}$	153	35	1.15	0.16

A. Velocity effect

When looking at the velocity effect on the RAO results (Fig. 8a), the magnitude clearly differs between both the velocities. Highest magnitude is noticed for the highest velocity, with a constant difference of more than $50\,\mathrm{W/(m/s)}$. That means that for the same amplitude of velocity fluctuation, the turbine power shows larger variations when the average flow velocity is higher. In addition, the frequency range where the RAO is defined is slightly larger for the highest velocity: until $f \simeq 0.4\,\mathrm{Hz}$ for $U_\infty = 1.0\,\mathrm{m/s}$ and $f \simeq 0.5\,\mathrm{Hz}$ for $U_\infty = 1.2\,\mathrm{m/s}$. This corresponds to what is shown on the coherence function in Fig. 7. The phase angle stays constant and always close to $0°$. It is not affected by the difference of the flow velocity.

B. Turbulence effect

Focusing on the effect of the turbulence intensity (Fig. 8b), decreasing the turbulence does not affect the RAO magnitude. The evolution of the RAO magnitude versus the frequency is similar between $I_\infty = 15$ and $1.5\,\%$. The frequency range where the RAO is defined is however twice as small as for $I_\infty = 1.5\,\%$ with a maximum frequency of $f \simeq 0.2\,\mathrm{Hz}$, comparing to $I_\infty = 15\,\%$. This is explained by the coherence function which is smaller in amplitude for $I_\infty = 1.5\,\%$ (not shown here) and by the cutoff which occurs for a lower frequency comparing to $I_\infty = 15\,\%$, as already observed by [18]. As previously observed, the phase angle stays constant and close to $0°$.

C. Wave-current effect

When comparing RAOs obtained for the two different wave-current conditions (Fig. 8c), the magnitude shows a similar trend as the previous one measured for $U_\infty = 1.0\,\mathrm{m/s}$, for frequencies lower than $0.5\,\mathrm{Hz}$. Some peaks clearly appear however for the highest frequencies with the main ones corresponding to the wave frequencies of 0.6 and $0.7\,\mathrm{Hz}$. Wave response is consequently visible on RAOs magnitude with values close to $250\,\mathrm{W/(m/s)}$ for wave at $0.6\,\mathrm{Hz}$ and close to $275\,\mathrm{W/(m/s)}$ for wave at $0.7\,\mathrm{Hz}$. According to this last result, the shortest wave ($0.7\,\mathrm{Hz}$) has a stronger impact on the turbine power fluctuation. It is worth noting that these two wave peaks are even higher in amplitude than the values observed for the lowest frequencies, corresponding to the largest turbulent structures in the flow. Again, the wave effect shows a stronger impact on the turbine power fluctuation than the turbulence. This impact is however focused on a narrow band of frequency, i.e. around the the wave frequency, on the contrary to the turbulence which affects the lowest frequencies from 0 to $0.5\,\mathrm{Hz}$. The phase angle stays again close to $0°$ for $f < 0.5\,\mathrm{Hz}$, but varies for the wave frequencies: $\varphi \simeq -120°$ for $f = 0.6\,\mathrm{Hz}$ and $\varphi \simeq -75°$ for $f = 0.7\,\mathrm{Hz}$. This phase variation depends on the distance d between the turbine rotor and the LDV measurement point. As explained in section II-B, this distance is time-compensated by removing the average time lag between both signals $u(t)$ and $P(t)$. However, this distance and its corresponding time lag does not correspond to an integer multiple of the wavelength of the chosen waves. That is the reason why a non-zero phase is shown between the wave orbital velocity component and the turbine power in the presented RAO.

The transfer functions of the turbine power obtained for all these various flow conditions are more or less similar, excepted for the flow velocity variation and for the wave frequency components. The quality of this method is questioned and discussed in the next section to verify its confidence level.

IV. DISCUSSION

A. Quality of the method

To check the accuracy and the robustness of the method, the RAO is processed using the same procedure as described in section II-B, on a repeated acquisition. Such repeated acquisition is especially useful in the highly turbulent flows to further investigate experimental uncertainties. The generated flow corresponds to a constant velocity of $U_\infty = 1.0\,\mathrm{m/s}$, with the wavemaker in position, i.e. immersed in the water, but inoperative (parked). This flow is quite similar to the one obtained downstream from a wall-mounted obstacle, which has been intensively described in [19], with large scale vortices shed downstream from the obstacle (wavemaker). The corresponding acquisitions are related to the database B (see table I). The results are shown on Fig. 9.

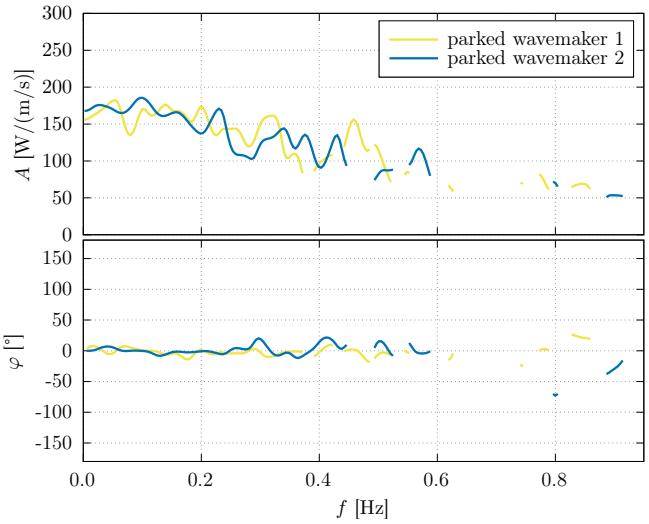

Fig. 9. RAO of the turbine power for $TSR = 4$ and for $U_\infty = 1.0\,\mathrm{m/s}$ with the parked wavemaker for two successive identical records

According to these results, the RAOs' magnitudes are quite similar to the previous ones presented on Fig. 8 for $U_\infty = 1.0\,\mathrm{m/s}$. The amplitude decreases when the frequency increases and values are quite identical. The blue and yellow curves are very close to each other as well (Fig. 9), but far from being identical when comparing their variations versus the frequency. For example, a peak is visible for the blue curve at $f = 0.22\,\mathrm{Hz}$ while nothing corresponds to that peak for the yellow curve at the same frequency. On the contrary, a sharp increase is noticeable for the yellow curve at $f = 0.45\,\mathrm{Hz}$ whereas the blue curve is undefined because the corresponding coherence function is lower than 0.5 for the same frequency. Finally, according to these observations, we can conclude the small amplitude variations noticed on the magnitude of the presented RAOs are not directly related to the response of the turbine in the flow. They can be attributed to the PSD processing, more especially the window size (2^{12}) or the overlapping ($50\,\%$), to the acquisition duration ($256\,\mathrm{s}$), to the sampling frequency ($128\,\mathrm{Hz}$) or to the convergence of the time series, mainly for turbulent flows. Because RAOs are only defined in the low frequency range, RAO results are better defined when acquisitions are longer and the convergence of the time series increases.

B. Generic transfer function determination

According to the previous results and observations, and supposing the turbine RAO is only dependent on the flow velocity, we try to define a generic response of the turbine power. All RAOs' magnitudes and phases, obtained for the same $U_\infty = 1.0\,\mathrm{m/s}$ are plotted together on Fig. 10 and fitted.

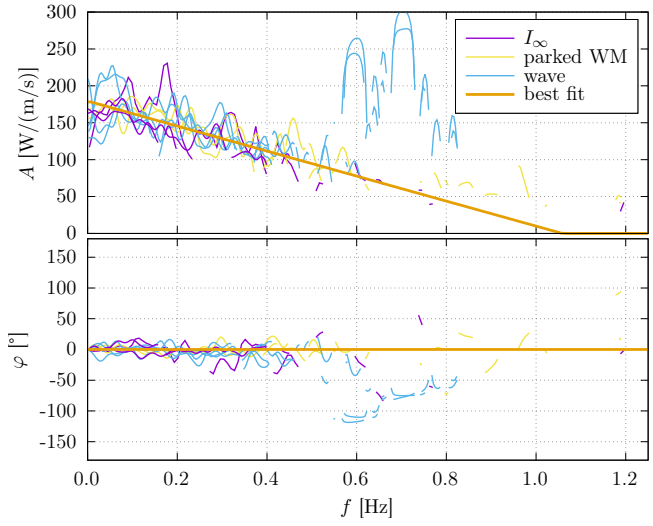

Fig. 10. RAO of the turbine power for every flow velocity case with $U_\infty = 1.0\,\mathrm{m/s}$ and the corresponding best fits for the magnitude and phase, without accounting for the wave peaks at 0.6 and $0.7\,\mathrm{Hz}$ for the wave cases

On this figure, results obtained for the two different turbulent rates as well as results obtained for the parked wavemaker as well as results obtained for the wave and current combinations and their corresponding repeated acquisitions are all plotted together. From this plot, a linear tendency clearly appears in the frequency range between 0 and $0.6\,\mathrm{Hz}$ for the magnitude. The highest peaks at $f = 0.6$ and $0.7\,\mathrm{Hz}$ (blue curves) corresponding to the wave response are not accounted for the processing of the least-squares regression depicted in orange. Finally, this best fit curve is expressed as:

$$A(f) = \begin{cases} -170 \times f + 180 & \text{if} \quad 0 < f \leq 180/170 \\ 0 & \text{if} \quad f > 180/170 \end{cases} \tag{7}$$

For the phase angle, because we noticed it is always close to zero, we impose:

$$\varphi(f) = 0, \forall f \tag{8}$$

Based on these two simple equations 7 and 8, we can first formulate the function $RAO(f)$ as expressed by equation 6. The turbine power fluctuations $P'(t)$ can then be reconstructed, based on a velocity measurement $u(t)$ using the following formula:

$$P'(t) = \mathcal{F}^{-1}[RAO(f) \times \mathcal{F}(u(t))] \tag{9}$$

C. Turbine power reconstruction

As an example, this reconstruction is applied on a particular flow condition for $U_\infty = 1.0\,\mathrm{m/s}$: the turbine (rotating at $TSR = 4$) is immersed in a bathymetry generated turbulence (see Fig. 11). This flow condition has not been used to process the generic turbine RAO previously determined. This flow is intensively described in [19] and its effect on the turbine is studied in [14], [20], [21]. As depicted in Fig. 11, two distances between the wall-mounted obstacle and the turbine rotor are tested: $16H$ and $23H$, with $H = 250\,\mathrm{mm}$ the obstacle height and $H \simeq D/3$.

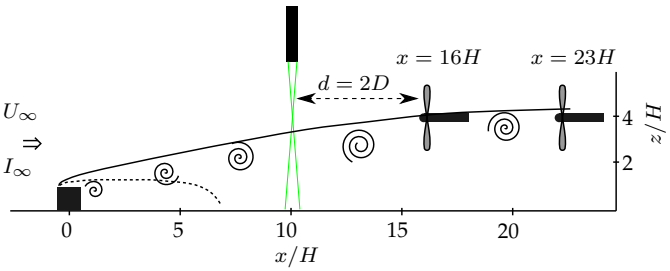

Fig. 11. Schematic representation of the experimental set-up with the obstacle and the turbine located at the two positions $x/H = [16; 23]$ in the obstacle wake extension. According to [19], the black line stands for the wake extension: $U = 0.9 \times U_\infty$ and the dotted line represents the recirculation zone: $U < 0$. The turbine is always centred at mid-depth ($z/H = 4$) and the LDV (only represented here when the turbine is at $16H$) is always located at $d = 2D$ upstream of the rotor.

An upstream velocity measurement is recorded during these experiments as well, with the LDV probe located at $d = 2D$ from the turbine rotor, i.e. at about $10H$ and $17H$ from the wall-mounted obstacle respectively. This velocity measurement is acquired in synchronization with the turbine parameters, so it is used to reconstruct the turbine power from the generic turbine RAO. The fluctuating part of the recorded velocity as well as the recorded and reconstructed power fluctuations are shown on Fig. 12 for both distances.

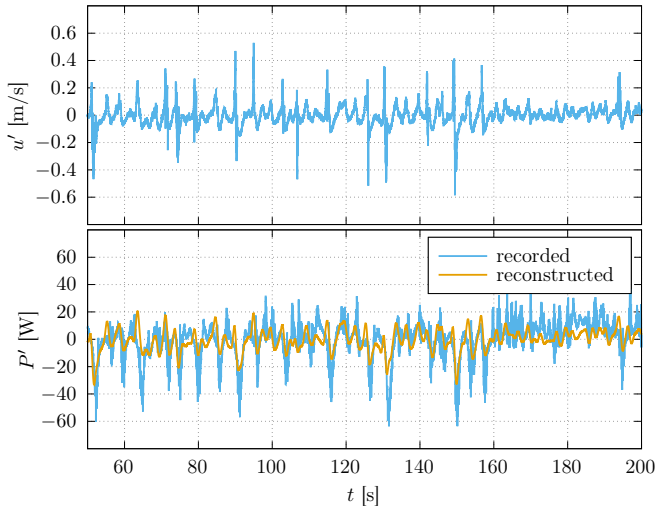

(a)

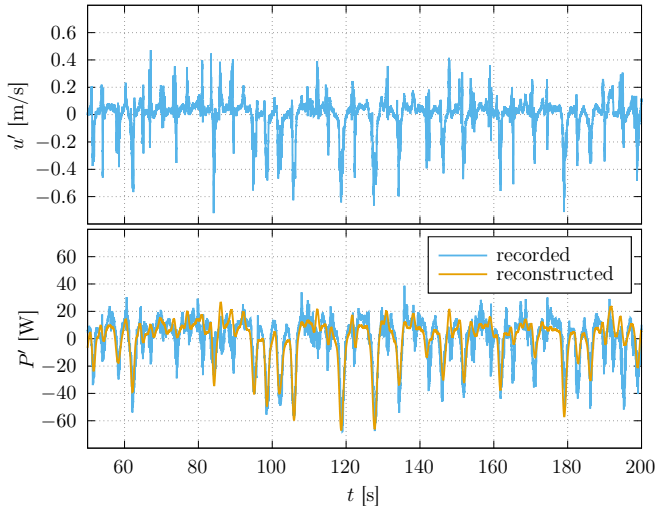

(b)

Fig. 12. Fluctuating part of the recorded upstream velocity and comparison of the corresponding recorded and reconstructed turbine power history, when the turbine is immersed in a bathymetry generated turbulence. Distances between the wall-mounted obstacle and the turbine rotor is $16H$ (a) and $23H$ (b). The corresponding correlation coefficients between both power signals are 0.57 for (a) and 0.80 for (b). The generic response defined in equations 7 and 8 from the least-squares regression is used as power turbine RAO.

The reconstructed response is very close to the recorded power fluctuation for the highest distance (Fig. 12b) but significantly differs for the shortest one (Fig. 12a). The corresponding correlation coefficients between both power signals are 0.57 and 0.80 for $16H$ and $23H$ respectively. Looking at the standard-deviation of the signals, we get the results summarized in table IV. For the shortest distance, value is lower for the reconstructed power with a difference of about $40\,\%$. On the contrary, the standard-deviation is very close for the highest distance. Such a difference on the reconstructed power between the turbine locations is explained by the evolution of the flow downstream from the wall-mounted obstacle. Such an evolution can generate some significant differences between the flow measured by the LDV and the flow perceived by the turbine located $2D \simeq 6H$ downstream from the velocity measurement point. As shown in [19], [21] and on Fig. 11 for this particular flow configuration, the wake of the obstacle is perceived from a distance of about $15H$ downstream from the obstacle at the turbine depth. For the shortest distance ($16H$), the turbine is consequently immersed in the wake but the flow velocity measurement is not, because its distance to the obstacle is about $10H$ only ($2D$ upstream of the rotor). On the contrary, for the highest distance ($23H$), both the turbine and the LDV probe are in the wake of the obstacle. As a result, the flow measured by the LDV is quite similar to the one perceived by the turbine. According to these last observations, when applying such a reconstruction from the turbine RAO, it is consequently important to use a flow velocity measurement acquired at the nearest possible position to where the turbine rotor is expected to be located. In addition, when determining the turbine RAO, a particular attention to the flow evolution has to be done for a better accuracy of the transfer function.

TABLE IV
STANDARD-DEVIATION OF THE RECORDED AND RECONSTRUCTED TURBINE POWER, EXPRESSED IN W

distance to the obstacle	$\sigma(P_{recorded})$	$\sigma(P_{reconstructed})$
$16H$	12.6	7.5
$23H$	15.4	15.7

Another reason explaining this difference is however linked to the frequency reconstruction of the turbine power with this method. Applying such a RAO method exactly corresponds to a low-pass filter, due to the coherence function threshold limiting the frequencies to the lowest ones only. As explain in section II-B, the turbine acts as a low-pass filter concerning its fluctuations, which follow those of the velocity in the low-frequency regime only [22]. This is clearly confirmed with Fig. 13 showing PSDs of the velocity and of the recorded and reconstructed turbine power for this particular flow example and for both turbine locations. As already observed by [22], the spectral functions of the turbine power show the existence of three distinct regions: a low-frequency regime in which power fluctuations follow those of the velocity, an intermediate regime, often coinciding with part of the inertial sub-range, in which the power fluctuation scale as $f^{-11/3}$, and a high-frequency regime containing the blade-passing frequency and harmonics. With the presented RAO method, only the first regime is fully reproduced. This corresponds to a linear response of the turbine parameter to the flow fluctuation which is provided by the coherence function (see Fig. 7) for the lowest frequencies only. As shown on Fig. 13 differences appear between the recorded and reconstructed PSDs from $f \simeq 0.5\,\mathrm{Hz}$ which roughly corresponds to the end of the first regime. To better reproduce the turbine response, and especially to better predict the power peaks, this RAO method needs to be improved, accounting for these highest frequencies.

Finally, this method could easily be coupled with a dynamic wake model (e.g. as presented in [23], [24]) representing the velocity fluctuations or the velocity

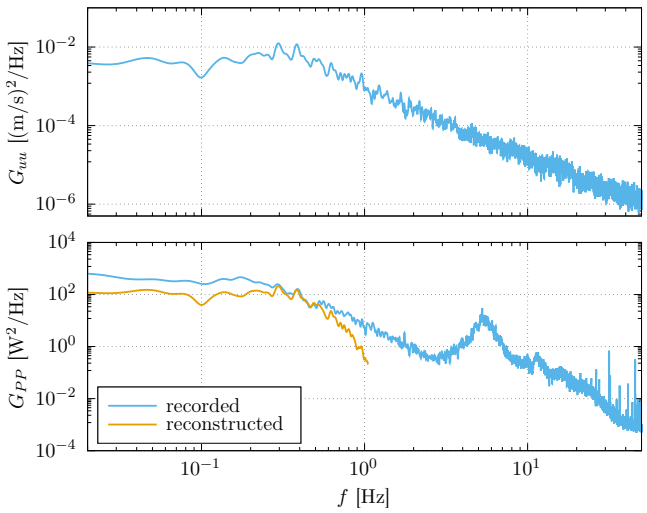

(a)

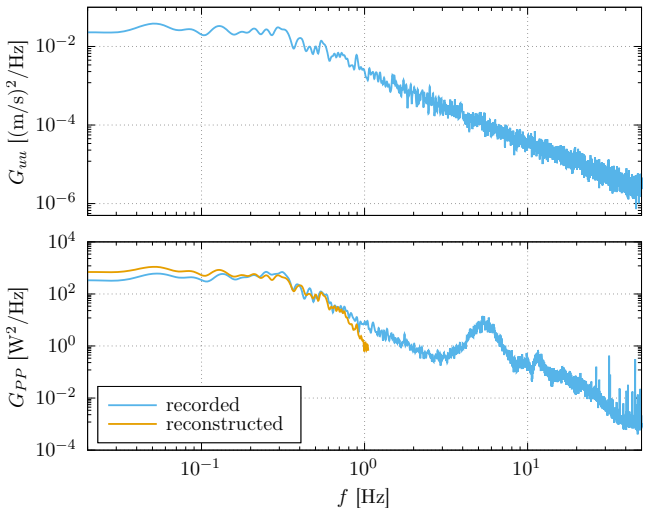

(b)

Fig. 13. PSDs of the incoming velocity and comparison of the PSDs of the recorded and reconstructed turbine power for the same corresponding cases as in Fig. 12

spectra measured in a turbine wake, to be extended to a tidal plant. The global power fluctuation of the plant linked to the site turbulence could then be predicted and anticipated for a better grid integration. In addition, this method constitutes a simple tool to predict the fluctuations of the turbine parameters (power, torque, thrust or blade forces) to better quantify the occurrence and the loading of extreme events, versus the incoming velocity variations.

V. Conclusion

A method is proposed in this study to predict the unsteady fluctuations of forces and moments of a tidal turbine, like power, torque, thrust or blade root forces. This method is based on a spectral analysis of the incoming flow velocity measurement and the considered turbine parameter, i.e. the power here, both acquired in synchronization. A corresponding turbine transfer function is established on a frequency range where the causality between these signals is proven using the coherence function. Because the coherence function only shows linearity between both signals for the lowest frequencies, the turbine transfer function is only valid on this low frequency regime, i.e. for $f \leq 1.0\,\mathrm{Hz}$. The transfer functions obtained for various flow configurations, i.e. velocities, turbulence rates and wave-current interactions, shows a decrease in its magnitude when the frequency increases. On the contrary, the corresponding phase stays constant and close to 0° whatever the frequency. A difference is observed in the magnitude when the flow velocity changes, with higher values for higher velocities. Peaks with high values corresponding to the wave frequency appear for the wave and current cases, showing the regular wave effect is locally higher on the turbine parameters fluctuations than turbulent structures. No significant variations is however noticed in the magnitude for $f \leq 0.6\,\mathrm{Hz}$ for a given flow velocity, whatever the turbulence rate. A least-squares regression of the various transfer function magnitudes and phases is proposed enables a generic turbine response to be defined. A reconstruction of the turbine power fluctuations is carried out on a particular turbulent flow with a bathymetry generated turbulence, using this generic response, based on the simultaneously acquired flow velocity upstream of the rotor. The accuracy of the reconstruction strongly depends on the flow conditions which must be the same than the one perceived by the turbine. A particular attention to this last point is furthermore required during the RAO determination when the turbine and the velocity measurement point have to be separated for an acquisition in synchronization. Improvement is however required accounting for the highest frequencies turbine response, particularly in the corresponding inertial sub-range of the flow velocity and for the regime containing the blade-passing frequency. This method should soon be applied on various type of tidal turbines: vertical and horizontal axis as well as rotors with various blade solidity. It should enable a comparison of the turbine response to the lowest frequencies variations of the flow to be carried out.

Bearing in mind these limits we have shown, this spectral transfer function model could be used for the structural design of a tidal turbine enabling the loading of the extreme events to be predicted and anticipated. Finally, coupling this model to a turbine wake model, power fluctuations of an entire tidal plant could be simulated and used for a better grid integration.

ACKNOWLEDGEMENT

The authors would like to thank Thomas Bacchetti from IFREMER for his assistance in this experimental work.

REFERENCES

[1] M. Harrold and P. Ouro, "Rotor loading characteristics of a full-scale tidal turbine," *Energies*, vol. 12, no. 6, pp. 1–19, 2019.

[2] P. Ouro and T. Stoesser, "Impact of Environmental Turbulence on the Performance and Loadings of a Tidal Stream Turbine," *Flow, Turbulence and Combustion*, vol. 102, no. 3, pp. 613–639, 2019.

[3] M. Allmark, R. Ellis, C. Lloyd, S. Ordonez-Sanchez, K. Johannesen, C. Byrne, C. Johnstone, T. O'Doherty, and A. Mason-Jones, "The development, design and characterisation of a scale model Horizontal Axis Tidal Turbine for dynamic load quantification," *Renewable Energy*, 2020. [Online]. Available: https://doi.org/10.1016/j.renene.2020.04.060

[4] M. Lewis, J. McNaughton, C. Márquez-Dominguez, G. Todeschini, M. Togneri, I. Masters, M. Allmark, T. Stallard, S. Neill, A. Goward-Brown, and P. Robins, "Power variability of tidal-stream energy and implications for electricity supply," *Energy*, vol. 183, pp. 1061–1074, 2019.

[5] J. Bossuyt, M. F. Howland, C. Meneveau, and J. Meyers, "Measurement of unsteady loading and power output variability in a micro wind farm model in a wind tunnel," *Experiments in Fluids*, vol. 58, no. 1, pp. 1–17, 2017.

[6] G. Pinon, M. F. Hurst, and E. Lukeba, "Semi-analytical estimate of energy production from a tidal turbine farm with the account of ambient turbulence," *International Journal of Marine Energy*, vol. 19, pp. 70–82, 2017.

[7] B. Gaurier, G. Germain, J.-V. Facq, and T. Bacchetti, "Wave and current flume tank of IFREMER at Boulogne-sur-mer. Description of the facility and its equipment," Ifremer, Tech. Rep., 2018.

[8] B. Gaurier, G. Germain, and G. Pinon, "How to correctly measure turbulent upstream flow for marine current turbine performances evaluation?" in *Advances in Renewable Energies Offshore - Proceedings of the 3rd International Conference on Renewable Energies Offshore, RENEW 2018*, 2019, pp. 23–30. [Online]. Available: https://archimer.ifremer.fr/doc/00461/57308/

[9] B. Gaurier, S. Ordonez-Sanchez, J.-v. Facq, G. Germain, C. Johnstone, R. Martinez, F. Salvatore, I. Santic, T. Davey, C. Old, and B. Sellar, "MaRINET2 Tidal Energy Round Robin Tests-Performance Comparison of a Horizontal Axis Turbine Subjected to Combined Wave and Current Conditions," *Journal of Marine Science and Engineering*, vol. 8, no. 6, p. 463, jun 2020. [Online]. Available: https://www.mdpi.com/2077-1312/8/6/463

[10] R. Martinez, B. Gaurier, S. Ordonez-Sanchez, J.-v. Facq, G. Germain, C. Johnstone, I. Santic, F. Salvatore, T. Davey, C. Old, and B. Sellar, "Tidal Energy Round Robin Tests: A Comparison of Flow Measurements and Turbine Loading," *Journal of Marine Science and Engineering*, vol. 9, no. 4, p. 425, apr 2021. [Online]. Available: https://www.mdpi.com/2077-1312/9/4/425

[11] L. P. Chamorro, S.-J. Lee, D. Olsen, C. Milliren, J. Marr, R. Arndt, and F. Sotiropoulos, "Turbulence effects on a full-scale 2.5 MW horizontal-axis wind turbine under neutrally stratified conditions," *Wind Energy*, vol. 18, no. 2, pp. 339–349, feb 2015. [Online]. Available: http://doi.wiley.com/10.1002/we.1700

[12] N. Tobin, H. Zhu, and L. P. Chamorro, "Spectral behaviour of the turbulence-driven power fluctuations of wind turbines," *Journal of Turbulence*, vol. 16, no. 9, pp. 832–846, sep 2015. [Online]. Available: http://www.tandfonline.com/doi/full/10.1080/14685248.2015.1031242

[13] Y. Jin, S. Ji, and L. P. Chamorro, "Spectral energy cascade of body rotations and oscillations under turbulence," *Physical Review E*, vol. 94, no. 6, p. 063105, dec 2016. [Online]. Available: https://link.aps.org/doi/10.1103/PhysRevE.94.063105

[14] B. Gaurier, M. Ikhennicheu, G. Germain, and P. Druault, "Experimental study of bathymetry generated turbulence on tidal turbine behaviour," *Renewable Energy*, vol. 156, pp. 1158–1170, aug 2020. [Online]. Available: https://linkinghub.elsevier.com/retrieve/pii/S0960148120306340

[15] P. Druault, B. Gaurier, and G. Germain, "Spatial integration effect on velocity spectrum: Towards an interpretation of the -11/3 power law observed in the spectra of turbine outputs," *Renewable Energy*, vol. 181, pp. 1062–1080, 2022.

[16] M. Anvari, G. Lohmann, M. Wächter, P. Milan, E. Lorenz, D. Heinemann, M. R. R. Tabar, and J. Peinke, "Short term fluctuations of wind and solar power systems," *New Journal of Physics*, vol. 18, no. 6, 2016.

[17] O. Faltinsen, *Sea loads on ships and offshore structures*. Cambridge university press, 1993.

[18] O. Durán Medina, F. G. Schmitt, R. Calif, G. Germain, and B. Gaurier, "Turbulence analysis and multiscale correlations between synchronized flow velocity and marine turbine power production," *Renewable Energy*, vol. 112, pp. 314–327, 2017.

[19] M. Ikhennicheu, G. Germain, P. Druault, and B. Gaurier, "Experimental study of coherent flow structures past a wall-mounted square cylinder," *Ocean Engineering*, vol. 182, no. May, pp. 137–146, 2019.

[20] M. Ikhennicheu, B. Gaurier, G. Germain, P. Druault, G. Pinon, and J.-V. Facq, "Experimental study of the wall-mounted cylinder wake effects on a tidal turbine behaviour compared to free stream turbulence," in *13th European Wave and Tidal Energy Conference*, Naples, Italy, 2019. [Online]. Available: https://ewtec.org/proceedings/

[21] B. Gaurier, P. Druault, M. Ikhennicheu, and G. Germain, "Experimental analysis of the shear flow effect on tidal turbine blade root force from three-dimensional mean flow reconstruction," *Philosophical Transactions of the Royal Society A: Mathematical, Physical and Engineering Sciences*, 2020.

[22] G. Deskos, G. S. Payne, B. Gaurier, and M. Graham, "On the spectral behaviour of the turbulence-driven power fluctuations of horizontal-axis turbines," *Journal of Fluid Mechanics*, vol. 904, p. A13, dec 2020. [Online]. Available: https://www.cambridge.org/core/product/identifier/S0022112020006813/type/journal{_}article

[23] W. H. Lam, L. Chen, and R. Hashim, "Analytical wake model of tidal current turbine," *Energy*, vol. 79, no. C, pp. 512–521, 2015. [Online]. Available: http://dx.doi.org/10.1016/j.energy.2014.11.047

[24] O. A. Lo Brutto, V. T. Nguyen, S. S. Guillou, J. Thiébot, and H. Gualous, "Tidal farm analysis using an analytical model for the flow velocity prediction in the wake of a tidal turbine with small diameter to depth ratio," *Renewable Energy*, vol. 99, pp. 347–359, 2016.